ELSEVIER

Journal of Inorganic Biochemistry 91 (2002) 312–319

JOURNAL OF Inorganic Biochemistry

www.elsevier.com/locate/jinorgbio

# $^{153}Sm^{3+}$ and $^{111}In^{3+}$ DTPA derivatives with high hepatic specificity: in vivo and in vitro studies

M.I.M. Prata[a,b,c], A.C. Santos[a], M. Neves[d], C.F.G.C. Geraldes[b,c,*], J.J.P. de Lima[a]

[a]*Serviço de Biofísica e Biomatemática, Faculdade de Medicina, Universidade de Coimbra, 3001-401 Coimbra, Portugal*
[b]*Departamento de Bioquímica, Faculdade de Ciências e Tecnologia, Universidade de Coimbra, Apartado 3126, 3001-401 Coimbra, Portugal*
[c]*Centro de Neurociências, Universidade de Coimbra, 3001-401 Coimbra, Portugal*
[d]*Instituto Tecnológico e Nuclear, 2686-953 Sacavém, Portugal*

Received 17 October 2001; received in revised form 4 February 2002; accepted 6 March 2002

**Abstract**

Two DTPA derivatives, a mono-amide derivative containing an iodinated synthon, DTPA-IOPsp ($L_1$) and the ligand DTPA(BOM)$_3$ (BOM=benzyloxymethyl) ($L_2$), radiolabelled with $^{153}Sm^{3+}$ and $^{111}In^{3+}$, were studied as potential hepatospecific gamma scintigraphic agents. In vivo studies with Wistar rats show that the main excretory pathway for all the chelates studied is the hepatobiliary system. The complexes of $L_2$ show even greater hepatobiliary specificity than $L_1$, perhaps as a consequence of longer blood circulation times due to their strong affinity towards HSA. The $^{153}Sm^{3+}$ chelates are also more hepatospecific than the corresponding $^{111}In^{3+}$ chelates. The $La^{3+}$ and $In^{3+}$ chelates of $L_1$ and $L_2$ show some structural and dynamic differences in aqueous solution, as studied by $^1H$ NMR spectroscopy. While only two nona-coordinated isomers were observed for the $La^{3+}$ complexes with both ligands, its number is much larger in the $In^{3+}$ complexes, with both octa- and hepta-coordinated species (with unbound side arms), as well as structural isomers for each coordination number. 

*Keywords:* Hepatic specificity; 153-Samarium; DTPA derivatives; 111-Indium

## 1. Introduction

Nuclides of indium-111 and samarium-153 have found widespread use in nuclear medicine. $^{153}Sm$ is a β- and γ-emitter with a half-life of 1.9 days [1], which is currently used in the common form of $^{153}$SmEDTMP (EDTMP stands for ethylenediamino-tetramethylenephosphonate) as a palliative agent for painful bone metastasis [2]. These two radionuclides present suitable chemical properties for in vivo applications: only the +3 oxidation state occurs in water and its aqueous chemistry is dominated by its strong Lewis acidity and oxophilicity [3].

The primary objective of our work was to perform biodistribution studies and obtain information about biokinetics, clearance and in vivo stability in Wistar rats of complexes of $^{153}Sm^{3+}$ and $^{111}In^{3+}$ with two DTPA derivatives, a mono-amide derivative containing an iopanoic acid as iodinated synthon, DTPA-IOPsp, {11,14,17-tris-(carboxymethyl)-1-(5-(1-carboxy-2-ethyl-propyl)-2,4,6-triiodo-phenyl)-2,9-bis-carbonyl-1,8,11,14,17-pentaaza}-nonadecan-19-oic acid ($L_1$), and DTPA(BOM)$_3$ (BOM=benzyloxymethyl), {4-carboxy-5,8-bis-(carboxymethyl)-1-phenyl-8,11-bis(1-carboxy-2-benzyloxymethyl-ethyl)-2-oxa-5,8,11-triaza}-tridecan-13-—oic acid ($L_2$) (see Fig. 1). Ligand $L_2$ was used as a mixture containing random populations of the absolute *R* and *S* configurations for the three chiral carbons present. The Gd(III) complexes of both ligands, which have already been characterised [4–6], show a high binding affinity to HSA, in particular $Gd^{3+}$–$L_2$ [6]. Furthermore, the $Gd^{3+}$–$L_1$ complex is preferentially eliminated via the hepatobiliary pathway (65% biliary elimination in rats after 8 h [4]). The established hepatobiliary contrast agents, Gd(BOPTA) (Multihance™, Bracco) and Gd(EOB-DTPA) (Eovist™, Schering), were found to undergo >35% biliary excretion and to enter the hepatocytes via a

*Corresponding author. Tel.: +351-2-3982-4531; fax: +351-2-3985-3607.
*E-mail address:* geraldes@ci.uc.pt (C.F.G.C. Geraldes).

0162-0134/02/$ – see front matter 
PII: S0162-0134(02)00417-8

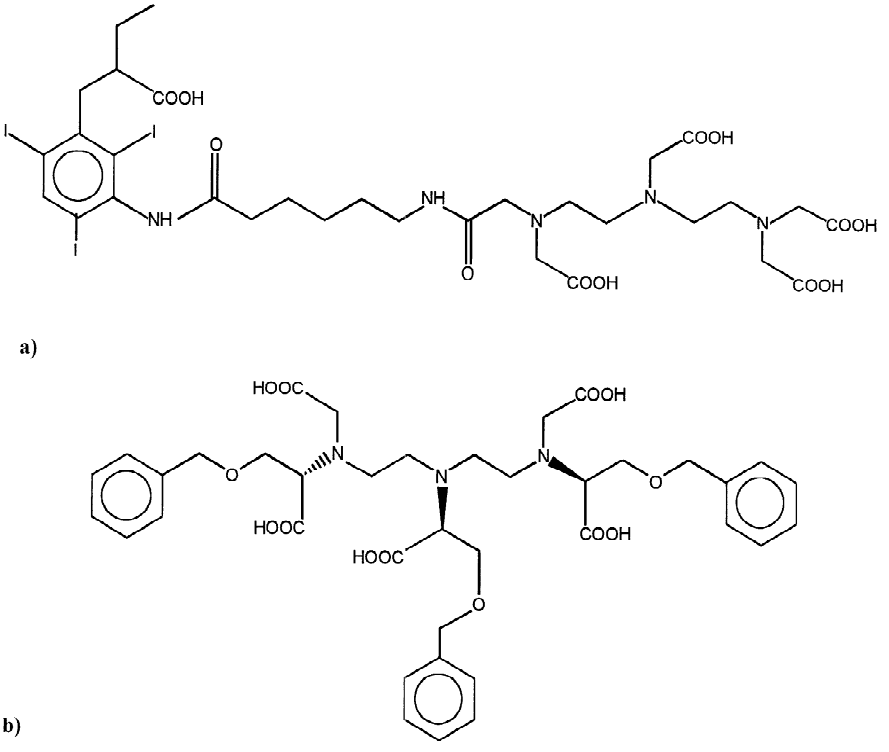


Fig. 1. Chemical structures of the ligands (a) $L_1$, (b) $L_2$.

combination of passive diffusion and a carrier-mediated mechanism [7–9], shared with conjugated bilirubin, and involving an organic anion transporter [10], which has been found to be the plasma membrane ABC protein cMOAT/mrp2 [11]. However, a recent study of the transport mechanism of $Gd^{3+}$–$L_1$ through hepatocytes indicates that its biliary excretion occurs via a different carrier-mediated pathway, in common with taurocholate but not conjugated bilirubin [9], operated by the human liver organic anion transporting polypeptide (OATP) [12]. The enhanced liver uptake of this compound is due to three main factors, the presence of the iopanoic acid moiety, the lipophilicity and the charge distribution on the molecule, but the presence of the iopanoic moiety is crucial [4]. However a contrast agent used in MRI should be administered in much higher concentrations than a radiopharmaceutical used in nuclear medicine. Since the in vivo behaviour of a complex can be metal- and dose-dependent, the current studies were undertaken in order to elucidate the relationships of structure and concentration with activity, which govern the biodistribution and pharmacokinetics of these metal chelates.

As far as we know, the $In^{3+}$ complexes of these two ligands have not yet been characterised. The different ionic radii of the $In^{3+}$ and $Ln^{3+}$ ions (0.81 Å for $In^{3+}$, 1.216 Å for $La^{3+}$ and 1.032 Å for $Lu^{3+}$ [13]) are reflected in the different coordination numbers of their polyaminocarboxylate complexes. In this work, the solution structures and dynamics of the $In^{3+}$–$L_1$, $In^{3+}$–$L_2$, $La^{3+}$–$L_1$ and $La^{3+}$–$L_2$ complexes are compared by $^1$H NMR. Any differences between the various metal complexes of the same ligand with the two ions may be reflected in different in vivo behaviour of their $^{153}Sm^{3+}$ and $^{111}In^{3+}$ complexes.

## 2. Experimental

### 2.1. Reagents and apparatus

$^{111}InCl_3$ in 0.8 N HCl (specific activity 0.4 GBq/ml) was obtained from CIS-Biointernational (Saclay, France). 153-Samarium oxide was produced at the ITN (Instituto Tecnológico e Nuclear), Lisbon with a specific activity >5 GBq/mg. The chromatographic paper used in the quality control (3MM Chr Whatman) was obtained from W.&R. Balston, UK. The two ligands used in this work were synthesized and characterised as described elsewhere [4,5] and kindly provided by Dr. P.A. Anelli from Bracco, Milan, Italy. Other reagents and solvents were obtained from either Aldrich or Sigma (Madrid, Spain) and used as received. All reagents to be used in vivo were prepared sterile and pyrogen free.

A gamma camera-computer system (GE 400 GenieAcq, from General Electrics, Milwaukee, USA) was used for acquisition and pre-processing. Data processing and display were performed on a personal computer using homemade software developed for the IDL 5.2 computer tool. A well-counter (DPC-Gamma $C_{12}$, LA, USA) with a

Compaq DeskPro compatible computer was used for activity counting in the biodistribution studies. The gamma camera has been previously calibrated for each radioisotope.

### 2.2. Preparation of 153-samarium oxide

The $^{153}$Sm oxide was prepared from a 98% enriched target, sealed into a quartz vial and welded into an aluminium can, by neutron irradiation using a thermal flux of $2.3\times10^{13}$ n/cm$^2$ s. Following irradiation the sample was opened, dissolved in 1 N HCl and brought to a stock concentration of $1.9\times10^{-3}$ M.

### 2.3. NMR studies

For the NMR studies, complexes were prepared in $D_2O$ (99.8% D) solutions at 5 mM concentrations, by adding stoichiometric amounts of the ligands to stock solutions of indium(III) nitrate and lanthanum(III) chloride. The pD of the solutions was adjusted with DCl and $CO_2$-free NaOD using a Crison MicropH 2002 pH-meter with an Ingold 405-M5 combined electrode (Crison Instruments, Barcelona, Spain) and converted to pH values using the isotopic correction pH=pD−0.4. $^1$H NMR spectra were recorded at 25 °C, on a Varian UNITY-500 spectrometer (Varian, Palo Alto, USA) at an external field of 11.8 T, operating at 499.84 Hz. The $^1$H resonance shifts were measured relative to the $^1$H water signal set at 4.74 ppm. Assignments of the proton NMR spectra were based on literature data for similar systems and in the results of two-dimensional homonuclear correlation spectra (COSY).

### 2.4. Partition coefficients

$^{111}InL_1$ was prepared in distilled water by mixing the ligand with $^{111}InCl_3$ (in a 10:1 molar ratio) and adjusting the pH to ca. 7 with 0.1 M NaOH. The partition coefficient was determined by addition of 25 μl of $^{111}In^{3+}$-chelate solution in a test tube containing 1 ml of saline solution and 1 ml of 1-octanol. The tubes were vortexed and centrifuged for 3 min at 3000 rev./min. Then, 100-μl aliquots of each phase were taken for radioactivity counting. The partition coefficients were calculated by dividing the net radioactivity counting of the organic phase by that of the aqueous phase. The results presented are the means of five determinations (with a S.D.<0.01).

### 2.5. Protein binding

Albumin solutions were freshly prepared by dissolving HSA in 0.1 M HEPES buffer to obtain 0.6 mM concentration (assuming 69 kDa as the HSA molecular weight [14]). $L_1$ and $L_2$ water solutions (0.2 mM) were labeled with a small amount of $^{111}InCl_3$ (in 0.1 N HCl), and then $InCl_3$ (non-radioactive) was added to obtain a 1:1 complex. These solutions were incubated with 2 ml of the HSA solution and were continuously stirred for 6 h at 37 °C and then left overnight at room temperature. Samples were finally ultrafiltrated through Centricon filters (from Amicon, France) and activity counted both in the ultrafiltrate and the protein bound portions. The percentage of protein bound compounds was calculated using the equation:

% protein bound

= 100 × [counts in labeled protein/

(counts in labeled protein + counts in ultrafiltrate)].

### 2.6. Gamma imaging

A stock solution of $^{153}SmCl_3$ was prepared by dissolving $^{153}Sm_2O_3$ in 0.1 M HCl. $^{111}InCl_3$ was used as received. Stock solutions of the ligands were prepared in isotonic HEPES pH ca. 7 buffer and mixed (in a 1:1 mole ratio, with 50% ligand excess) with the metal chlorides. The final pH was adjusted to 7.0 with diluted solutions of NaOH. The radiochemical purity was determined by chromatography using 3MM Whatman chromatography paper developed with a mixture of $NH_3$/EtOH/$H_2O$ (in the ratio 0.1 ml/2 ml/4 ml, respectively) analysing 2 μl of each solution of the complex. With this system, the free metal ion stays at the origin while the labelling product migrates to $R_f$=0.9. The dried strips were cut into 1 cm pieces and counted in a γ well counter. For all the complexes, the percentage of bound metal averaged 98%.

Gamma images and the biological distribution were determined for all the complexes using 300-g Wistar rats. All animal studies were carried out in compliance with procedures approved by the appropriate institutional review committees. Conscious rats were allowed free access of food and water ad libitum. Four groups of three animals (one group for each complex) were anaesthetised with ketamine (50 mg/ml)/chloropromazine (2.5%) (10:3).

#### 2.6.1. $^{153}$SmL studies

Wistar rats were injected in the femoral vein with ca. 400 μCi of the respective $^{153}Sm^{3+}$ chelate. The animals were positioned in dorsal decubitus over the detector.

#### 2.6.2. $^{111}$InL studies

Wistar rats were injected in the femoral vein with ca. 150 μCi of the respective $^{111}In^{3+}$ chelate. The animals were positioned in ventral decubitus over the detector.

For both the radionuclides, image acquisition was initiated immediately before radiotracer injection. Sequences of 180 images (10 s each) were acquired to 64×64 matrices.

In order to analyse the transport of radiotracer over time, five regions of interest (RI) were drawn on the image files, corresponding to the thorax, liver, brain, intestines and left kidney. From these RI, time–activity curves were obtained

using an IDL-based program (Interactive Data Language, Research Systems, Boulder, CO, USA), which enables the RI's drawing and calculates the activity per pixel–time curves. In addition, static data were acquired at 24 and 48 h after the radiotracer injection.

### 2.7. Biodistribution experiments

Groups of four animals were injected in the femoral vein with ca. 100 μCi of the two $^{111}In^{3+}$ or $^{153}Sm^{3+}$ complexes and sacrificed 5, 15 and 30 min later. The major organs were removed, weighed and counted in a γ well counter. Similar biodistribution studies were also performed with the rats referred to in the previous section sacrificed at 48 h.

## 3. Results and discussion

### 3.1. NMR studies

Since the complexes of the whole series of lanthanide ions with a variety of DTPA derivatives are isostructural [15–17], the diamagnetic $La^{3+}$–L complexes were chosen (instead of the paramagnetic $Sm^{3+}$–L complexes) to study their structure and dynamics in aqueous solution by $^{1}H$ NMR, and compare with the corresponding $In^{3+}$–L chelates. The spectra (excluding the aromatic region) of the 1:1 complexes at pH 7.0 are shown in Fig. 2. Assignments were based on published results on similar systems [15–18] and on the two-dimensional homonuclear correlation spectra (COSY) obtained (see Fig. 1S in Supporting information).

The spectra of the $La^{3+}$–$L_1$ and $In^{3+}$–$L_1$ complexes (Fig. 2a and c, respectively) are fairly similar, but the latter is sharper. Assuming that the $La^{3+}$–$L_1$ complex is $[La(DTPA\text{-}IOPsp)(H_2O)]^{-}$ and the ligand is bound as DTPA or DTPA bis-amides [15–18], the $La^{3+}$ ion is nona-coordinated, by the three amine nitrogen atoms, five oxygen atoms of the carboxylates and the amide carbonyl group, and one oxygen of the water molecule, forming a tri-capped trigonal prismatic coordination polyhedron. Two chiral centers are present in the ligand backbone (the central nitrogen and the terminal one next to the amide group), leading to a maximum of two diastereomeric pairs of enantiomers, and two observable sets of proton resonances. This is observed in the spectrum of $La^{3+}$–$L_1$, where many of the proton signals from the amide sub-

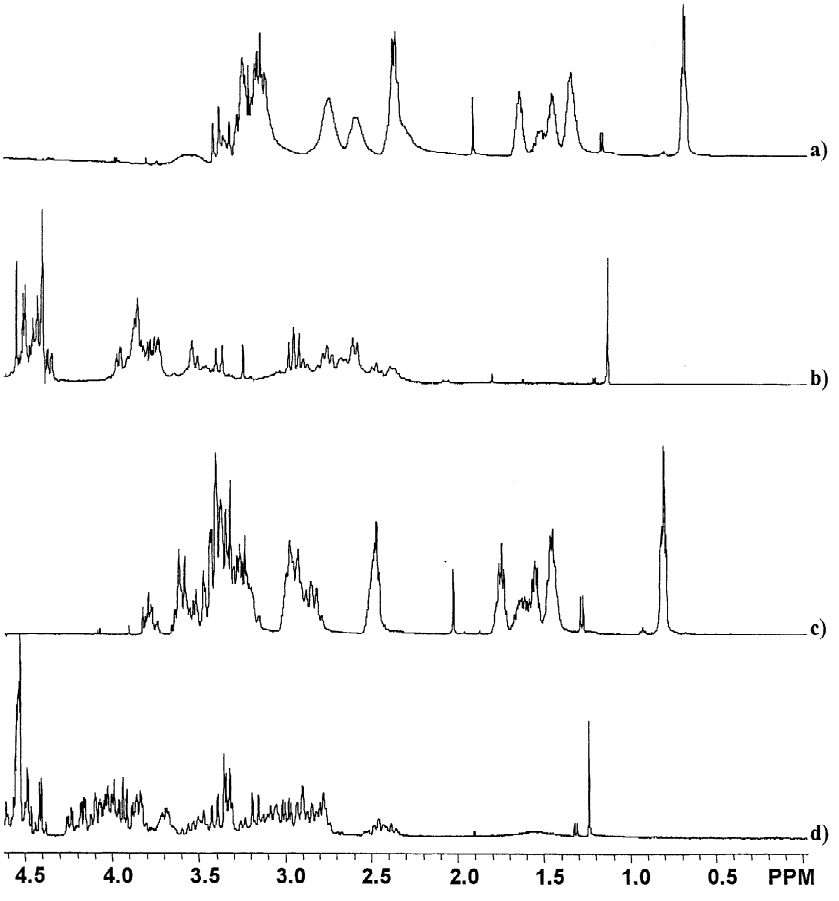


Fig. 2. $^{1}H$ NMR spectra of the 1:1 complexes in $D_2O$. Metal and ligand concentration 10 mM, pH 7.0: (a) $La^{3+}$–$L_1$, (b) $La^{3+}$–$L_2$, (c) $In^{3+}$–$L_1$, (d) $In^{3+}$–$L_2$.

stituent group are doubled, such as those of the iopanoic acid moiety, as shown by the COSY spectrum. The shift differences observed for the same protons in the two diastereomers of such a diamagnetic complex are very small. At least seven AB patterns are also seen in the 3.8–3.2 ppm region, corresponding to the five bound acetate and amide methylene groups of the ligand, as defined by their COSY cross-peaks [18]. The observation of broad resonances for the eight $CH_2$ protons of the ligand backbone (at 2.8–2.3 ppm) and for two of the AB patterns of acetate methylene groups (at 3.7–3.5 ppm) indicates that the dynamics of the interchange of the isomers present in the complex, e.g. by racemization of the central nitrogen [16], is relatively slow.

The $In^{3+}$–$L_1$ spectrum (Fig. 2c) shows at least two signals for each proton of the amide substituent group, but its aromatic proton, instead of a sharp singlet, has four components, two intense and two weaker. Many more acetate and amide $CH_2$ proton AB patterns, at 3.8–3.2 ppm, and backbone $CH_2$ sharp multiplets, at 3.4–2.8 ppm, are observed than in the spectrum of $La^{3+}$–$L_1$. All these observations indicate that the isomeric equilibrium is more complex in $In^{3+}$–$L_1$ than in $La^{3+}$–$L_1$, with both octa- and hepta-coordinated (with an unbound amide or acetate side arm) species, as well as structural isomers for each coordination number, giving multiple signals of different intensities for each proton. This is in agreement with previous studies of $In^{3+}$-DTPA-bis(amides) [18].

The complexity of the spectra of the $La^{3+}$–$L_2$ and $In^{3+}$–$L_2$ complexes (Fig. 2b and d) makes a detailed analysis impossible, even with COSY spectra. They are sharp but quite different, indicating structural differences. If the $La^{3+}$–$L_2$ complex is $[La(DTPA\text{-}(BOM)_3)(H_2O)]^{2-}$, with the ligand bound as DTPA or DTPA bis-amides [15–18], again with a nona-coordinated $La^{3+}$ ion in a tri-capped trigonal prismatic coordination polyhedron, the ligand backbone has three chiral centers (the three nitrogens), originating a maximum of four diastereomeric pairs of enantiomers [16]. Fast racemization of the middle nitrogen usually leads to four resonances at room temperature for each type of proton. The chirality in the benzyloxymethyl (BOM) chains originates another three chiral centers and a total of 32 diastereomeric pairs of enantiomers. The corresponding multiplication of signals is usually not observable in the NMR spectra of diamagnetic complexes, due to the very small proton shift differences, as is the case for the $[Ln(BOPTA)(H_2O)]^{2-}$ (BOPTA≡ DTPA-(BOM)) complexes [19].

The $La^{3+}$–$L_2$ spectrum (Fig. 2b) shows five distinct regions, corresponding to the different types of ligand protons. The aromatic moieties give multiple signals, indicating the presence of various isomers. The COSY spectrum (see Supporting information) allows assignment of some resonances, such as two intense AB patterns, corresponding to the $CH_2$ protons at the non-substituted bound acetate arms. This clearly indicates that only two major isomers (out of the four possible) are present in solution for this chelate. The $CH_2$ protons of the BOM groups directly attached to the α carbons at the substituted acetate arms, coupled to the α CH protons, give five different pairs of coupled quartets (AB parts of ABX systems), while the BOM $CH_2$ protons next to the benzene ring give at least eight singlet resonances (two major ones). This large number of resonances indicates that the chirality at the α carbons may affect the shifts of those protons, located very close to the chirality center.

The $In^{3+}$–$L_2$ spectrum (Fig. 2d) is very complex (up to 40 COSY cross-peaks), making any quantitative interpretations impossible. The observation of at least three major AB patterns from the $CH_2$ protons at the non-substituted bound acetate arms, and the large number (at least 17) of resonances for the backbone and BOM $CH_2$ protons close to the benzene ring, show that the number of major isomers is larger and/or more asymmetric than for the $La^{3+}$ complex. The $In^{3+}$ complex again has both octa- and hepta-coordinated species, as well as various isomers for each coordination number.

### *3.2. 1-Octanol/saline partition coefficients and interaction with HSA*

$^{111}In^{3+}$–$L_1$ and $^{153}Sm^{3+}$–$L_1$ give, at pH 7, an octanol/water log *P* value of −1.65 and −1.15, indicating a low lipophilicity for these complexes. Given the high hepatobiliary excretion observed for these chelates (see later), this result illustrates once again that lipophilicity is not the main factor determining the excretion pathway of a substance. One would expect high log *P* values for the complexes of $L_2$, as a consequence of the presence of the three aromatic groups in its chelates, but this value was −2.60 for $^{153}Sm^{3+}$–$L_2$ and was not determined experimentally for $^{111}In^{3+}$–$L_2$.

The complexes of $^{111}In^{3+}$ with both ligands bind efficiently to HSA, as shown by the values obtained for the percentage of protein-bound $In^{3+}$ chelates, 92% for $^{111}In^{3+}$–$L_1$ and 97% for $^{111}In^{3+}$–$L_2$. Although these values might be slightly overestimated, and perhaps need confirmation by other methodologies, they are in qualitative agreement with literature HSA binding data for the $Gd^{3+}$ complexes of these ligands. It has been reported that $Gd^{3+}$–$L_1$ binds strongly to human serum [4], and the values reported in the literature for the association constants of the $Gd^{3+}$ complexes to HSA are quite high: $K_a = 4.8\times10^3$ $M^{-1}$ for the $Gd^{3+}$–$L_1$ complex [20] and especially $K_a = 4.0\times10^4$ $M^{-1}$ for the $Gd^{3+}$–$L_2$ complex [6], a value quite similar to that of MS-325 [21]. In fact, binding of $Gd^{3+}$ complexes to HSA has been promoted by the presence of hydrophobic synthons of known high affinity to the serum proteins. An example is a series of DTPA- and DOTA-like complexes bearing iopanoic acid residues linked through an amidic bond [20], such as

$Gd^{3+}$–$L_1$, which is formulated as [Gd(DTPA-IOPsp)$(H_2O)]^{2-}$, where the presence of the long aliphatic spacer, a hydrophobic moiety and a negative charge contribute to their high affinity to HSA. Another example is the series of DTPA- and DOTA-like complexes with one, two or three benzyloxymethyl (BOM) groups attached, such as [Gd(DTPA-BOM)$(H_2O)]^{2-}$ (Gd(BOPTA)) or $Gd^{3+}$–$L_2$ ([Gd(DTPA-BOM)$_3(H_2O)]^{2-}$, where increasing number of BOM substituents and increasing negative charge of the chelate has been found to increase the affinity of the chelates to HSA [20,22]. Therefore, in what concerns these factors, the affinity of the above two families of $Gd^{3+}$ chelates to HSA has been optimised in the chelates of the $L_1$ and $L_2$ ligands used in the present study [20].

### 3.3. Gamma imaging

The values of the mean activity/pixel obtained from dynamic acquisitions for each region of interest (RI) after injection of the complexes, after background deduction, were used to obtain regional time–activity curves. The brain activity/pixel was considered as the background activity. Fig. 3 represents the averaged time–activity curves, normalised relative to the maximum activity, obtained for the complexes.

Rapid and complete liver uptake of $^{153}Sm^{3+}$ or $^{111}In^{3+}$ complexes of $L_1$ and $L_2$ was evident in the first 3 min post-injection. Subsequently, the chelates began to transit to the intestines. These gamma imaging studies demonstrate a similar behaviour of all the four complexes, although it has been very difficult to delineate each region accurately, due to the small size of the animals and some overlapping of the organs (e.g. intestines and left kidney). In some of the images some activity at the bladder level was noticed, which means that there is a concomitant kidney excretion. As discussed in the previous section, the high affinity of $Gd^{3+}$–$L_1$ and especially of $Gd^{3+}$–$L_2$ to the plasma protein human serum albumin (HSA) has been demonstrated [6,20], and as a consequence of this, one would expect a somewhat longer blood retention time for the complexes of $L_2$ relative to $L_1$. Although the peak of activity in the liver region occurs almost at the same time (3 to 6 min after injection) for all the $^{111}In^{3+}$ and $^{153}Sm^{3+}$ chelates, its decay is much slower for the complexes of $L_2$, and the onset of their transit through the intestines is also delayed. The renal profiles illustrate the appearance of a late (at about 1500 s) activity peak for the $In^{3+}$–$L_2$ complex. All these observations suggest a slightly longer lifetime of the $M^{3+}$–$L_2$ complexes in the bloodstream.

### 3.4. Biodistribution studies

The results of the animal biodistribution studies of $^{153}Sm^{3+}$–$L_1$, $^{153}Sm^{3+}$–$L_2$, $^{111}In^{3+}$–$L_1$ and $^{111}In^{3+}$–$L_2$ at 5, 15 and 30 min after injection of the radioactive chelates are summarised in Fig. 4. At 60 min after injection all the four complexes had almost cleared all tissues (data not shown), but one can notice some differences between them at earlier times. All the chelates are preferentially excreted by the hepatobiliary pathway (stated as the sum of liver

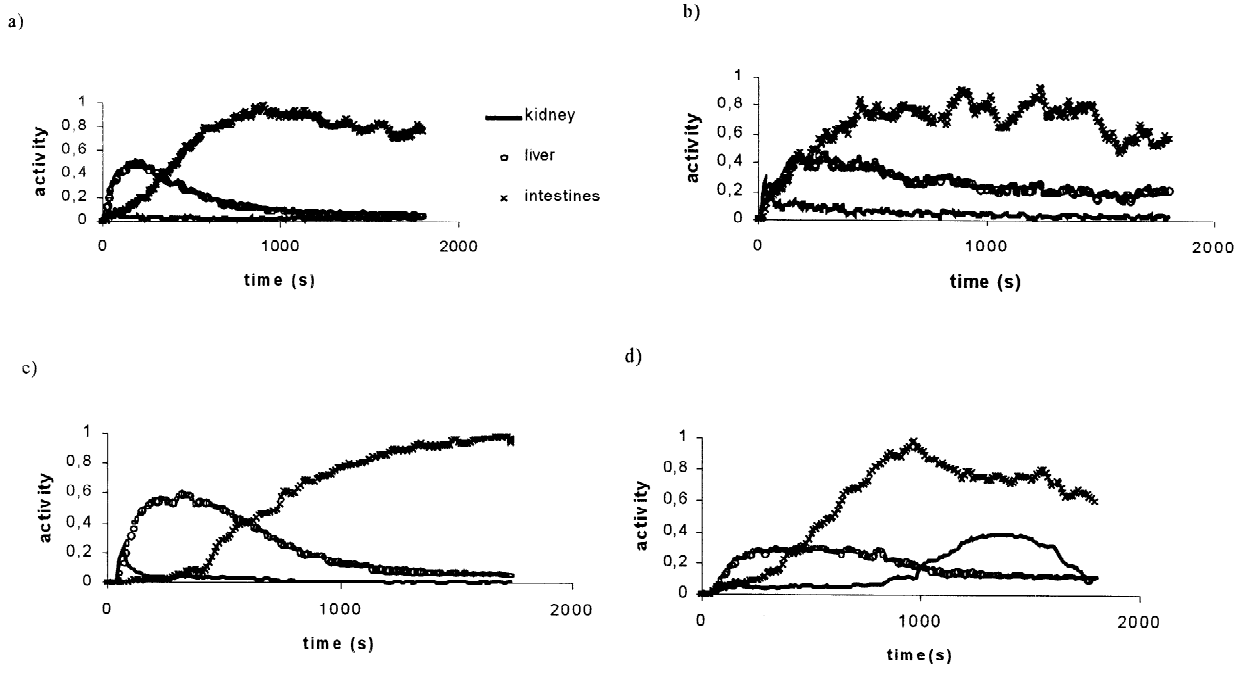


Fig. 3. Activity–time curves at the various regions of interest for (a) $^{153}SmL_1$; (b) $^{153}SmL_2$; (c) $^{111}InL_1$; (d) $^{111}InL_2$. *Y* axis represents normalized activity for the maximum curve counts.

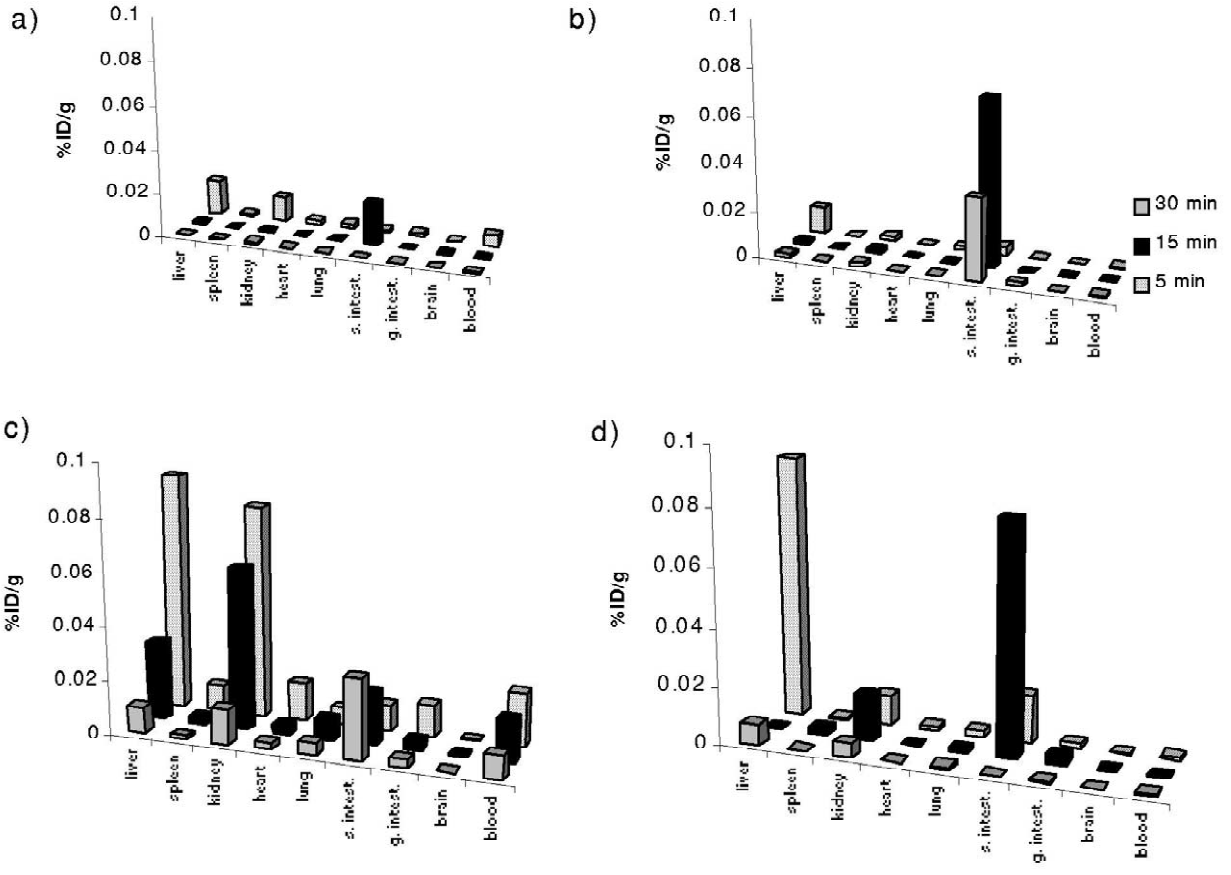


Fig. 4. Biodistribution of $^{153}$Sm and $^{111}$In chelates, obtained 5, 15 and 30 min after injection of: (a) $^{153}SmL_1$, (b) $^{153}SmL_2$, (c) $^{111}InL_1$, (d) $^{111}InL_2$. S.D.<5%.

and intestines), with a contribution greater than 60% in all cases, but kidney excretion has also a strong contribution in $^{111}In^{3+}$–$L_1$. The results above agree with the literature report for $Gd^{3+}$–$L_1$ [4]. The greater hepatobiliary specificity of $M^{3+}$–$L_2$ when compared with $M^{3+}$–$L_1$ is also evident from Fig. 4. The $^{153}Sm^{3+}$ chelates are also more hepatospecific than the corresponding $^{111}In^{3+}$ chelates, in particular for the $L_1$ complex. This might be a consequence of structural differences between the $Sm^{3+}$ and $In^{3+}$ complexes, as observed by NMR for the $La^{3+}$ and $In^{3+}$ complexes.

Fig. 4 also shows that $^{153}Sm^{3+}$–$L_2$ remains in the hepatobiliary system for slightly longer periods when compared with $^{153}Sm^{3+}$–$L_1$, in agreement with the previous information that $Gd^{3+}$–$L_2$ binds more strongly to HSA than $Gd^{3+}$–$L_1$ [6,20]. Although it is known that $Gd^{3+}$–$L_1$ is highly hepatospecific [4], the stronger affinity of $Gd^{3+}$–$L_2$ towards HSA retards its renal uptake to such an extent that its liver uptake is even higher than that of $Gd^{3+}$–$L_1$. In the case of the $^{111}In^{3+}$ complexes, $^{111}In^{3+}$–$L_1$ has a very different behaviour from $^{111}In^{3+}$–$L_2$: it remains longer in the blood, has a high renal uptake and both hepatobiliary and renal clearance mechanisms are quite slow. This might again be a consequence of structural differences between the $Sm^{3+}$ and $In^{3+}$ complexes.

From the imaging and biodistribution studies we can conclude that all the complexes were excreted quite quickly and preferentially via the hepatobiliary pathway. The total activity present in the different organs 48 h after injection of each of the four complexes was irrelevant (<0.0004% ID). However some late deposition of activity at the hepatosplenic region suggests some metal loss by the four chelates investigated. This may illustrate the need for the hepatospecific agents, which enter the hepatocytes and are subject to transmetallation reactions from strong chelating agents like ATP, to be more stable than the extracellular agents. However, no radioactivity was detected at the animal skeleton related with premature decomplexation of the metal complex [23].

## 4. Supporting information

Fig. 1S: COSY spectra of the 1:1 complexes (10 mM:10 mM metal and ligand concentration, pH 7.0) in $D_2O$. (a)

$La^{3+}$–$L_1$, (b) $La^{3+}$–$L_2$, (c) $In^{3+}$–$L_1$, (d) $In^{3+}$–$L_2$. Ordering information is given on any current masthead page.

## Acknowledgements

The authors thank Bracco S.p.A., Milan, Italy, for providing samples of the ligands, Dr. P.L. Anelli for useful discussions, Foundation of Science and Technology (F.C.T.) Portugal (Project Praxis 2/2.2/SAU/1194/95) and BIOMED II (MACE Project) of the E.U., for financial support. This work was carried out within the COST Chemistry D8 and D18 projects of the E.U.

## References

[1] N.E. Holde, Table of Isotopes, Handbook of Chemistry and Physics, 1990.
[2] W.F. Goeckeler, B. Edwards, W.A. Wolkert, J. Simon, D. Wilson, J. Nucl. Med. 28 (1987) 495–504.
[3] R.D. Hancock, A.E. Martell, Chem. Rev. 89 (1989) 1875–1914.
[4] P.L. Anelli, L. Calabi, C. de Haën, F. Fedeli, P. Losi, M. Murru, F. Uggeri, Gazz. Chim. Ital. 126 (1996) 89–97.
[5] F.M. Cavagna, F. Maggioni, P.M. Castelli, M. Dapra, L.G. Imperatori, V. Lorusso, B.G. Jenkins, Invest. Radiol. 32 (1997) 780–796.
[6] S. Aime, M. Chiaussa, G. Digilio, E. Gianolio, E. Terreno, J. Biol. Inorg. Chem. 4 (1999) 744–766.
[7] O. Clement, A. Muhler, V. Vexeler, Y. Berthezene, R.C. Brasch, Invest. Radiol. 27 (1992) 612–619.
[8] C. de Haën, V. Lorusso, F. Luzzani, P. Tirone, Acad. Radiol. 2 (1995) 232–238.
[9] L. Pascolo, F. Cupelli, P.L. Anelli, V. Lorusso, M. Visigalli, F. Uggeri, O. Tiribelli, Biochem. Biophys. Res. Commun. 257 (1999) 746–752.
[10] R.P.J. Oude Elferink, P.L.M. Jansen, Pharmacol. Ther. 64 (1994) 77–97.
[11] C.D. Klaassen, J.B. Watkins, Pharmacol. Rev. 36 (1984) 1–15.
[12] G.A. Kullak-Ublick, U. Beuers, C. Fahney, B. Hagenbuch, P.J. Meier, G. Paumgartner, Hepatology 26 (1997) 991–997.
[13] R.D. Shannon, Acta Cryst. A32 (1976) 751–767.
[14] T. Peters Jr., Adv. Prot. Chem. 37 (1986) 161–245.
[15] C.F.G.C. Geraldes, A.M. Urbano, M.C. Alpoim, M.A. Hoefnagel, J.A. Peters, J. Chem. Soc. Chem. Commun. (1991) 656–658.
[16] C.F.G.C. Geraldes, A.M. Urbano, M.A. Hoefnagel, J.A. Peters, Inorg. Chem. 32 (1993) 2426–2432.
[17] C.F.G.C. Geraldes, A.M. Urbano, M.C. Alpoim, A.D. Sherry, K.T. Kuan, R. Rajagolapan, F. Maton, R.N. Muller, Magn. Res. Imag. 13 (1995) 401–420.
[18] C.F.G.C. Geraldes, R. Delgado, A.M. Urbano, J. Costa, F. Jasanada, F. Nepveu, J. Chem. Soc. Dalton Trans. (1995) 327–335, and references therein.
[19] F. Uggeri, S. Aime, P.L. Anelli, M. Botta, M. Brocchetta, C. de Haën, G. Ermondi, M. Grandi, P. Paoli, Inorg. Chem. 34 (1995) 633–642.
[20] S. Aime, M. Fasano, E. Terreno, M. Botta, in: A.E. Merbach, É. Tóth (Eds.), The Chemistry of Contrast Agents in Medical Magnetic Resonance Imaging, Wiley, Chichester, 2001, pp. 193–241.
[21] R.B. Lauffer, D.J. Parmalee, S.U. Dunham, H.S. Ouellet, R.P. Dolan, S. Witte, T.J. McMurry, R.C. Walowitch, Radiology 207 (1998) 529–538.
[22] S. Aime, M. Botta, M. Fasano, S. Geninatti Crich, E. Terreno, J. Biol. Inorg. Chem. 1 (1996) 312–319.
[23] S.R. Vallabhajosula, J.F. Harwig, J.K. Siemsen, W. Wolf, J. Nucl. Med. 21 (1980) 650–656.